Supporting Information

Single Mo$_1$ (W$_1$, Re$_1$) Atoms Anchored in Pyrrolic-N$_3$ Doped Graphene as Efficient Electrocatalysts for the Nitrogen Reduction Reaction

Wanghui Zhao,[†a] Lanlan Chen,[†a] Wenhua Zhang [*ab] and Jinlong Yang [*a]

[a] *Hefei National Laboratory for Physical Sciences at the Microscale, and Synergetic Innovation Centre of Quantum Information & Quantum Physics, University of Science and Technology of China, Hefei, Anhui 230026, China.*

[b] *CAS Key Laboratory of Materials for Energy Conversion, University of Science and Technology of China, Hefei, Anhui 230026, China*

† These authors contributed equally.

* Corresponding Author

Email: *whhzhang@ustc.edu.cn;*
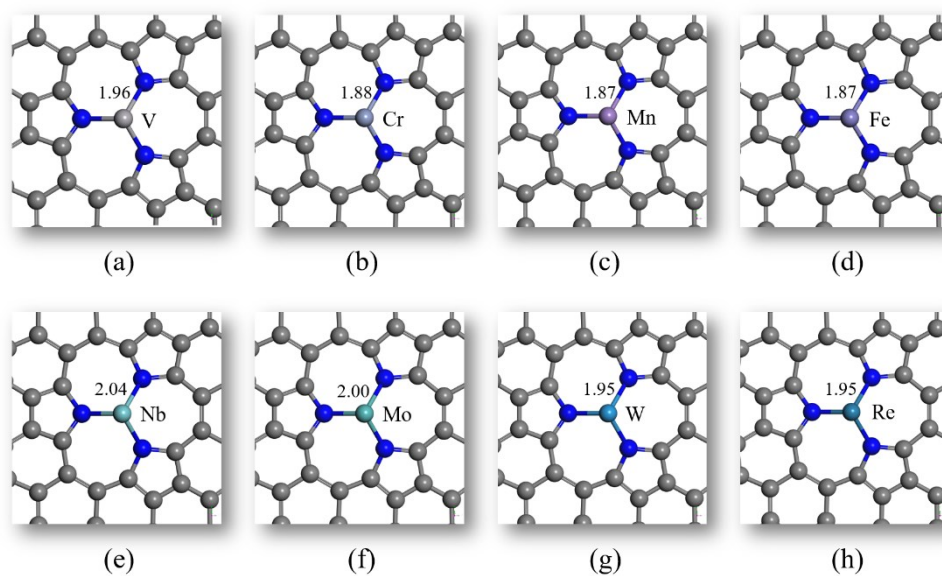
jlyang@ustc.edu.cn.

Results and Discussion

(a) (b) (c) (d)

(e) (f) (g) (h)

Fig. S1 From (a) to (h) are the structures of V_1, Cr_1, Mn_1, Fe_1, Nb_1, Mo_1, W_1 and Re_1 anchored at the center of pyrrolic-N_3 on graphene. The corresponding bond lengths between metal atoms and the pyrrolic-N are labeled in the adjacent blank. The gray, blue spheres represent carbon and nitrogen atoms, respectively.

Table S1. The total binding energies of M_1 atom anchored at the active center of pyrrolic-N_3–G.

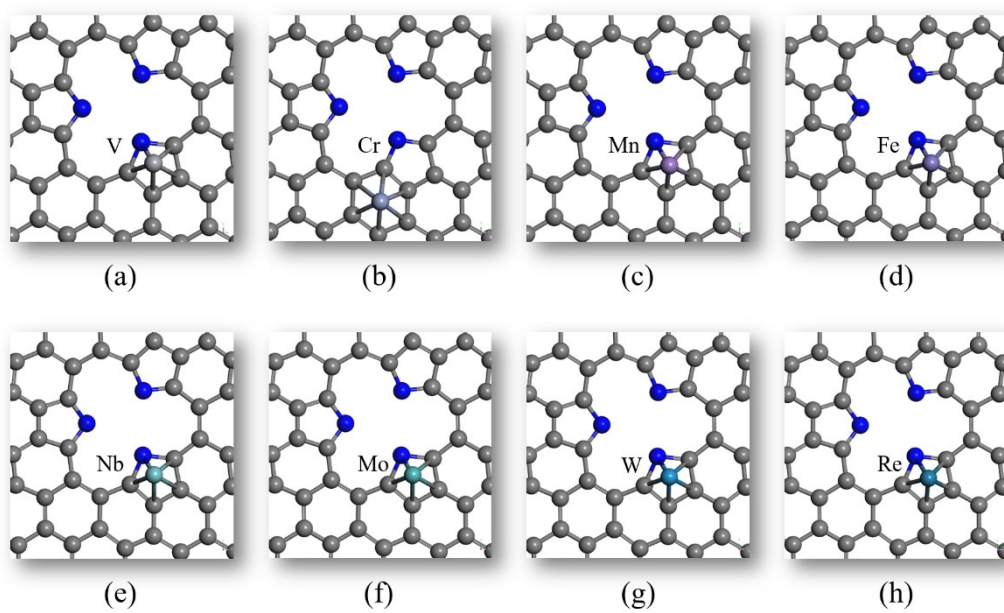| Doped metal	V	Cr	Mn	Fe	Nb	Mo	W	Re
E_b (eV)	9.99	6.92	6.49	8.07	9.14	7.26	6.09	4.29

Fig. S2 From (a) to (h) are the structures of V_1, Cr_1, Mn_1, Fe_1, Nb_1, Mo_1, W_1 and Re_1 anchored at the neighboring carbon sites on graphene. The corresponding metal atoms are labeled in the adjacent blank. The gray, blue spheres represent carbon and nitrogen atoms, respectively.
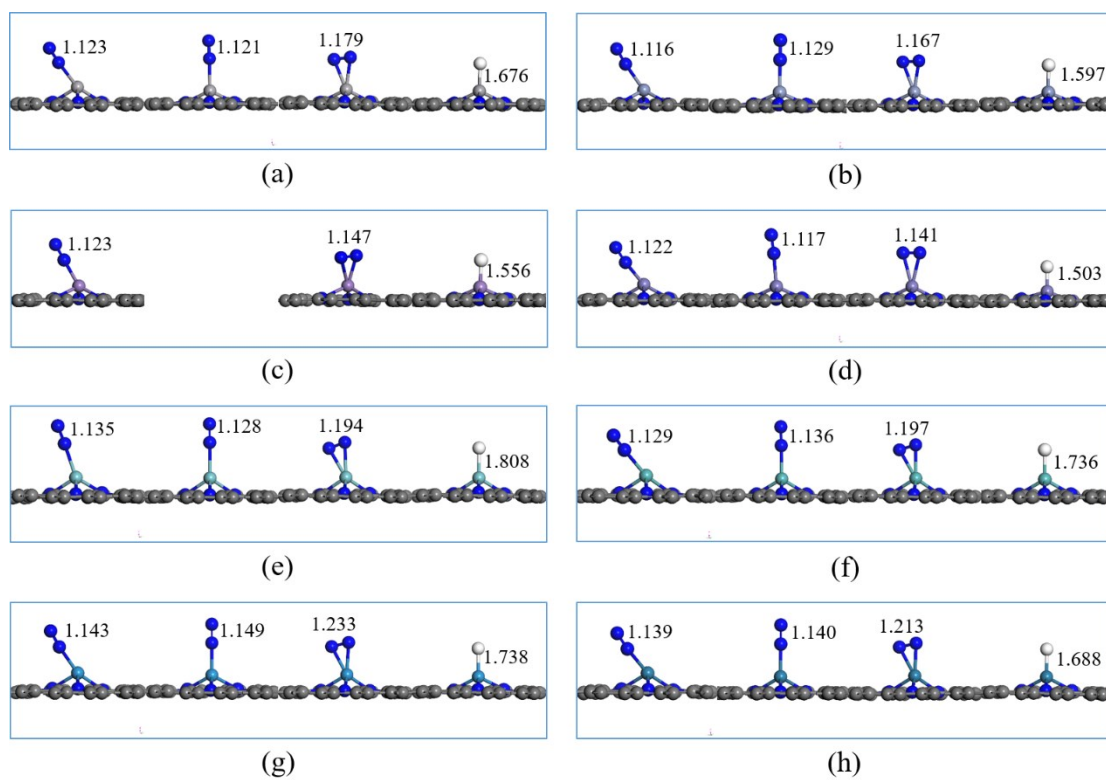
Fig. S3 From (a) to (h) are the optimized structures of N_2 (end-on and side on modes) and H adsorbed on $V_1(Cr_1,$ $Mn_1,$ $Fe_1,$ $Nb_1,$ $Mo_1,$ W_1 and Re_1)/pyrrolic-N_3-G. The bond lengths of N-N and M_1-H are marked next to each other. The gray, blue and white spheres represent carbon, nitrogen and hydrogen atoms, respectively.

Table S2. The calculated energy differences ($\triangle E$) between inclined and vertical configuration when N_2 adsorbed with end-on mode on each M_1/pyrrolic-N_3-G.

Doped metal	V	Cr	Fe	Nb	Mo	W	Re
$\triangle E$ (eV)	0.05	0.08	0.55	0.26	0.13	-0.06	0.12

Table S3. The calculated adsorption Gibbs free energy of atomic hydrogen and nitrogen molecule with end-on and side-on modes on each M_1/pyrrolic-N_3-G.

Doped metal	V	Cr	Mn	Fe	Nb	Mo	W	Re
$\triangle G_H$ (eV)	-0.07	0.29	-0.08	0.64	-0.17	-0.07	-0.58	-0.94
$\triangle G_{N2\text{-end-on}}$ (eV)	-0.25	-0.05	-0.32	-0.29	-0.28	-0.45	-0.49	-0.71
$\triangle G_{N2\text{-side-on}}$ (eV)	0.25	0.46	0.21	0.66	-0.10	-0.22	-0.63	-0.38

Table S4. The reaction Gibbs free energies of the adsorption Gibbs free energies of the second ($\triangle G_{N2\text{-}N2}$) and third dinitrogen ($\triangle G_{2N2\text{-}N2}$) molecules combined with the adsorption free energies of hydrogen with the presence of one ($\triangle G_{N2\text{-}H}$) and two dinitrogen ($\triangle G_{2N2\text{-}H}$) on each M_1/pyrrolic-N_3-G.

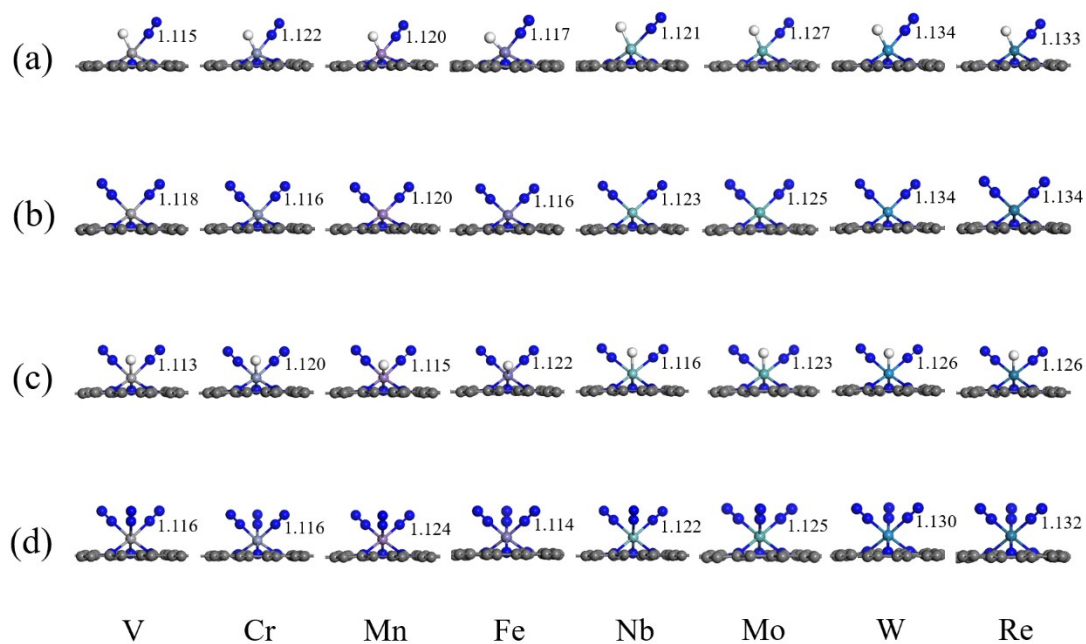| Doped metal	V	Cr	Mn	Fe	Nb	Mo	W	Re
Numbers of adsorbed N_2	3	2	3	3	3	3	3	3
$\Delta G_{N2\text{-}H}$ (eV)	0.43	0.84	0.42	0.75	0.23	0.22	-0.17	-0.51
ΔG_{2N2} (eV)	-0.12	-0.09	-0.21	-0.17	-0.18	-0.32	-0.25	-0.53
$\Delta G_{2N2\text{-}H}$ (eV)	0.73	1.14	0.59	0.56	0.40	0.57	0.22	0.12
ΔG_{3N2} (eV)	-0.10	0.01	-0.18	-0.17	-0.18	-0.16	-0.17	-0.51

Fig. S4 The optimized structures of side view with corresponding bond length of N-N. (a) optimized structures of *N_2-H. (b) optimized structures of *$2N_2$. (C) optimized structures of *$2N_2$-H. (d) optimized structures of *$3N_2$. The * represent the substrate of V_1(Cr_1, Mn_1, Fe_1, Nb_1, Mo_1, W_1 and Re_1)/pyrrolic-N_3-G. The gray, blue and white spheres represent carbon, nitrogen and hydrogen atoms, respectively.

Table S5. The calculated adsorption energy of N_2 (ΔE_{N_2}) and H_2O with the effect of hydrogen bond (E_{ad}^b) on M_1/pyrrolic-N_3-G, where the M_1 represents the single transition metal.

Species	E_{ad}^b (eV)	ΔE_{N_2} (eV)
V_1/pyrrolic-N_3-G	-0.48	-0.74
Cr_1/pyrrolic-N_3-G	-0.35	-0.56
Mn_1/pyrrolic-N_3-G	-0.50	-0.81
Fe_1/pyrrolic-N_3-G	-0.43	-0.81
Nb_1/pyrrolic-N_3-G	-0.31	-0.66
Mo_1/pyrrolic-N_3-G	-0.35	-0.82
W_1/pyrrolic-N_3-G	-0.50	-1.09
Re_1/pyrrolic-N_3-G	-0.67	-1.31

Table S6. The numbers of nitrogen molecules effectively binding on M_1/pyrrolic-N_3-G, the reaction Gibbs free energy (eV) of the formation of $*2N_2$-NNH (ΔG_{*NNH}), the adsorption free energy of $*3N_2$-H (ΔG_{M1-H}) and the potential difference (ΔU) between the formation of $*2N_2$-NNH and $*3N_2$-H ($\Delta U = U_{*NNH} - U_{M1-H} = - \Delta G_{*NNH} /e - [-\Delta G_{M1-H}/e]$) .

Doped metal	V	Cr	Mn	Fe	Nb	Mo	W	Re
number	3	2	3	3	3	3	3	3
ΔG_{*NNH}	1.22	1.13	1.01	1.76	0.77	0.49	0.33	0.51
ΔG_{M-H}	1.46	1.14	0.74	0.96	0.69	0.68	0.57	0.97
ΔU (V)	0.24	0.01	-0.27	-0.80	-0.08	0.19	0.24	0.46

Table S7. Reaction Gibbs free energy (eV) of each elementary step of NRR on $3N_2$-Mo_1/pyrrolic-N_3-G via distal, alternating and hybrid mechanisms with two speculator dinitrogen molecules. Here the * represents the substrate of $2N_2$-Mo_1/pyrrolic-N_3-G.

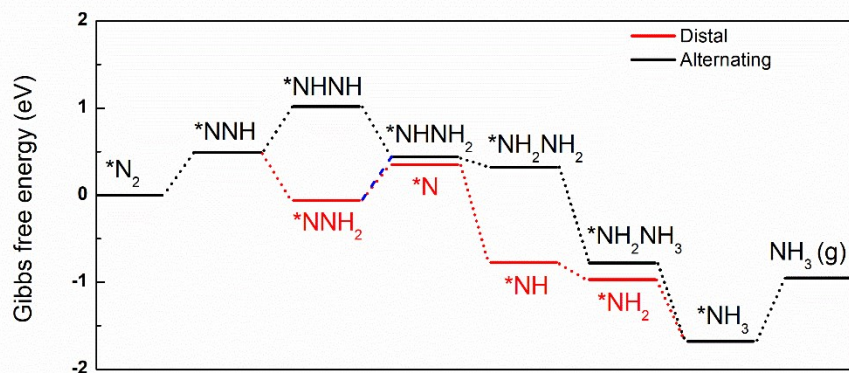| Distal	*NNH	*NNH$_2$	*N	*NH	*NH$_2$	*NH$_3$	NH$_3$
ΔG (eV)	0.49	-0.55	0.41	-1.12	-0.20	-0.71	0.73
Alternating	*NNH	*NHNH	*NHNH$_2$	*NH$_2$NH$_2$	*NH$_2$NH$_3$	*NH$_3$	NH$_3$
ΔG (eV)	0.49	0.53	-0.58	-0.12	-1.10	-0.90	0.73
Hybrid	*NNH	*NNH$_2$	*NHNH$_2$	*NH$_2$NH$_2$	*NH$_2$NH$_3$	*NH$_3$	NH$_3$
ΔG (eV)	0.49	-0.55	0.50	-0.12	-1.10	-0.90	0.73

Fig. S5 The calculated Gibbs free energy diagram of the two paths (Distal and Alternating) of NRR for $3N_2$-Mo_1/pyrrolic-N_3-G. The dotted blue line represents the hybrid path, here the * represents the substrate of $2N_2$-Mo_1/pyrrolic-N_3-G.

Table S8. Reaction Gibbs free energy (eV) of each elementary step of NRR on $3N_2$-W_1/pyrrolic-N_3-G via distal, alternating and hybrid mechanisms with two speculator dinitrogen molecules. Here the * represents the substrate of $2N_2$-W_1/pyrrolic-N_3-G.

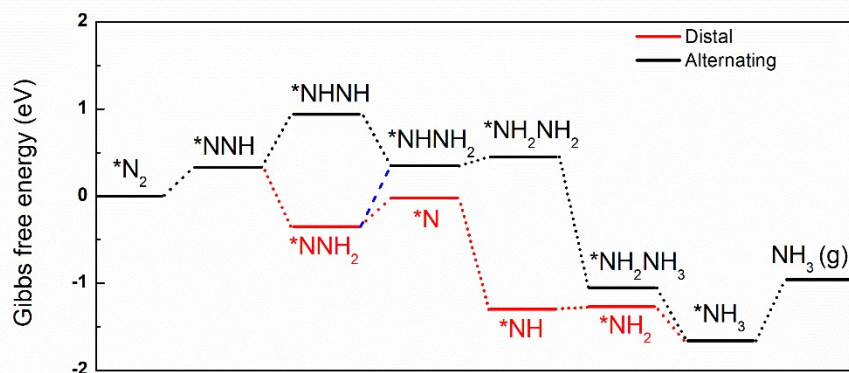| Distal	*NNH	*NNH$_2$	*N	*NH	*NH$_2$	*NH$_3$	NH$_3$
ΔG (eV)	0.33	-0.68	0.33	-1.28	0.03	-0.39	0.70
Alternating	*NNH	*NHNH	*NHNH$_2$	*NH$_2$NH$_2$	*NH$_2$NH$_3$	*NH$_3$	NH$_3$
ΔG (eV)	0.33	0.61	-0.59	0.10	-1.50	-0.61	0.70
Hybrid	*NNH	*NNH$_2$	*NHNH$_2$	*NH$_2$NH$_2$	*NH$_2$NH$_3$	*NH$_3$	NH$_3$
ΔG (eV)	0.33	-0.68	0.70	0.10	-1.50	-0.61	0.70

Fig. S6 The calculated Gibbs free energy diagram of the two paths (Distal and Alternating) of NRR for $3N_2$-W_1/pyrrolic-N_3-G. The dotted blue line represents the hybrid path, here the * represents the substrate of $2N_2$-W_1/pyrrolic-N_3-G.

Table S9. Reaction Gibbs free energy (eV) of each elementary step of NRR on $3N_2$-Re_1/pyrrolic-N_3-G via distal, alternating and hybrid mechanisms with two speculator dinitrogen molecules. Here the * represents the substrate of $2N_2$-Re_1/pyrrolic-N_3-G.

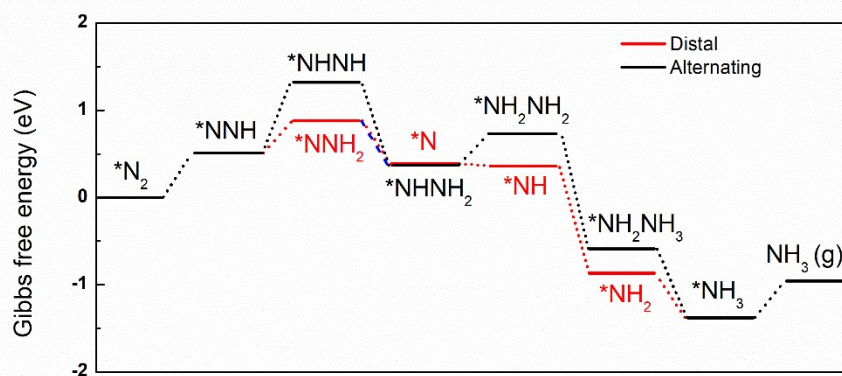| Distal	*NNH	*NNH$_2$	*N	*NH	*NH$_2$	*NH$_3$	NH$_3$
ΔG (eV)	0.51	0.37	-0.49	-0.03	-1.23	-0.51	0.42
Alternating	*NNH	*NHNH	*NHNH$_2$	*NH$_2$NH$_2$	*NH$_2$NH$_3$	*NH$_3$	NH$_3$
ΔG (eV)	0.51	0.81	-0.95	0.36	-1.32	-0.79	0.42
Hybrid	*NNH	*NNH$_2$	*NHNH$_2$	*NH$_2$NH$_2$	*NH$_2$NH$_3$	*NH$_3$	NH$_3$
ΔG (eV)	0.51	0.37	-0.51	0.36	-1.32	-0.79	0.42

Fig. S7 The calculated Gibbs free energy diagram of the two paths (Distal and Alternating) of NRR for $3N_2$-Re_1/pyrrolic-N_3-G. The dotted blue line represents the hybrid path, here the * represents the substrate of $2N_2$-Re_1/pyrrolic-N_3-G.

(a)

*NHNH   *NHNH$_2$ *NH$_2$NH$_2$ *NH$_2$NH$_3$

(b)

*NHNH   *NHNH$_2$ *NH$_2$NH$_2$ *NH$_2$NH$_3$

(c)

*NHNH   *NHNH$_2$ *NH$_2$NH$_2$ *NH$_2$NH$_3$

Fig. S8 The optimized intermediate configurations of NHNH, NHNH$_2$, NH$_2$NH$_2$ (N$_2$H$_4$) and NH$_2$NH$_3$ adsorbed on 2N$_2$-Mo$_1$/pyrrolic-N$_3$-G (a), 2N$_2$-W$_1$/pyrrolic-N$_3$ –G (b) and 2N$_2$-Re$_1$/pyrrolic-N$_3$-G (c) with top and side view, where the * represents the substrate of 2N$_2$-M$_1$/pyrrolic-N$_3$-G.

Table S10. The calculated spin moments of $3N_2$-M_1/pyrrolic-N_3-G. (M_1=V, Cr, Mn, Fe, Nb, Mo, W and Re)

Spin moments (μB)	metal	total	N-N	N-N	N-N
V_1/pyrrolic-N_3-G	2.10	2.79	-0.012/0.110	-0.012/0.111	-0.012/0.110
Cr_1/pyrrolic-N_3-G	2.18	2.55	-0.026/0.030	-0.026/0.029	none
Mn_1/pyrrolic-N_3-G	0.21	0.23	-0.005/0.001	-0.005/0.001	-0.005/0.001
Fe_1/pyrrolic-N_3-G	0.00	0.00	0.000/0.000	0.000/0.000	0.000/0.000
Nb_1/pyrrolic-N_3-G	1.26	2.64	-0.009/0.168	-0.009/0.168	-0.009/0.167
Mo_1/pyrrolic-N_3-G	1.08	1.81	-0.020/0.087	-0.020/0.087	-0.020/0.087
W_1/pyrrolic-N_3-G	0.96	1.90	-0.020/0.125	-0.020/0.125	-0.020/0.125
Re_1/pyrrolic-N_3-G	0.11	0.21	-0.003/0.013	-0.003/0.013	-0.003/0.013

Table S11. Reaction Gibbs free energy (eV) of each elementary step of NRR on $3N_2$-W_1/pyridine-N_3-G via distal, alternating and hybrid mechanisms with two speculator dinitrogen molecules. Here the * represents the substrate of $2N_2$-W_1/pyridine-N_3-G.

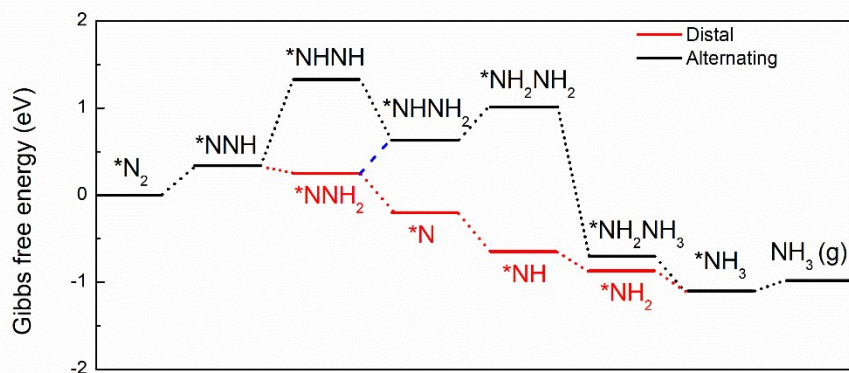| Distal	*NNH	*NNH$_2$	*N	*NH	*NH$_2$	*NH$_3$	NH$_3$	*N$_2$-H
ΔG (eV)	0.34	-0.09	-0.45	-0.45	-0.22	-0.20	0.12	0.43
Alternating	*NNH	*NHNH	*NHNH$_2$	*NH$_2$NH$_2$	*NH$_2$NH$_3$	*NH$_3$	NH$_3$	
ΔG (eV)	0.34	0.99	-0.70	0.38	-1.71	-0.40	0.12	
Hybrid	*NNH	*NNH$_2$	*NHNH$_2$	*NH$_2$NH$_2$	*NH$_2$NH$_3$	*NH$_3$	NH$_3$	ΔU
ΔG (eV)	0.34	-0.09	0.42	0.38	-1.71	-0.40	0.12	0.09 (V)

Fig. S9 The calculated Gibbs free energy diagram of the two paths (Distal and Alternating) of NRR for $3N_2$-W_1/pyridine-N_3-G. The dotted blue line represents the hybrid path, here the * represents the substrate of $2N_2$-W_1/pyridine-N_3-G.

Table S12. The calculated reaction free energy of key intermediates on $Mo_1(W_1, Re_1)$/pyrrolic-N_3-G by using the functional methods of PW91 and RPBE as the benchmark compared with PBE.

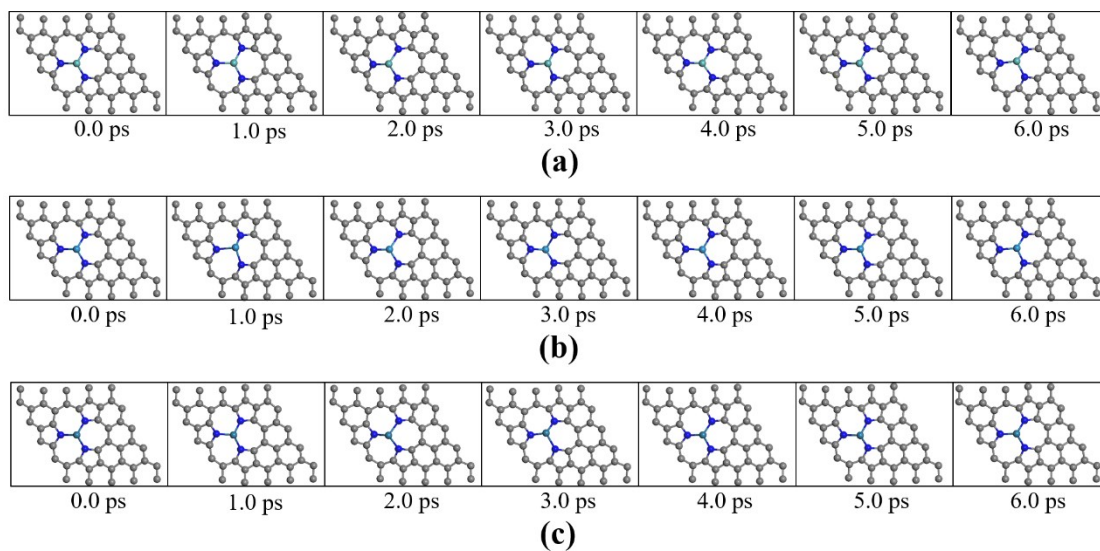| Species	Mo_1/pyrrolic-N_3-G (ΔG, eV)			W_1/pyrrolic-N_3-G (ΔG, eV)			Re_1/pyrrolic-N_3-G (ΔG, eV)		
	PBE	PW91	RPBE	PBE	PW91	RPBE	PBE	PW91	RPBE
*H	-0.07	-0.05	-0.05	-0.58	-0.67	-0.43	-0.94	-0.97	-0.84
*2H	0.10	0.14	0.45	0.13	-0.09	-0.06	0.56	0.53	0.46
*N_{2_end-on}	-0.45	-0.38	-0.41	-0.49	-0.63	-0.46	-0.71	-0.84	-0.78
*N_2-H	0.22	0.24	0.43	-0.17	-0.27	-0.36	-0.51	-0.47	-0.47
*$2N_2$	-0.32	-0.27	-0.22	-0.25	-0.38	-0.53	-0.53	-0.67	-0.71
*$2N_2$-H	0.57	0.61	0.50	0.22	0.12	0.05	0.12	0.07	0.01
*$3N_2$	-0.16	-0.11	-0.23	-0.17	-0.39	-0.49	-0.51	-0.69	-0.67
*$3N_2$-H	0.68	0.66	0.47	0.57	0.51	0.34	0.97	0.92	0.60
*$2N_2$-NNH	0.49	0.46	0.46	0.33	0.28	0.31	0.51	0.49	0.47

Fig. S10 The calculated AIMD simulations to investigate the stability of Mo_1/pyrrolic-N_3-G (a), W_1/pyrrolic-N_3-G (b) and Re_1/pyrrolic-N_3-G (c) at 400 K by seven sets of snapshots for 6 ps.
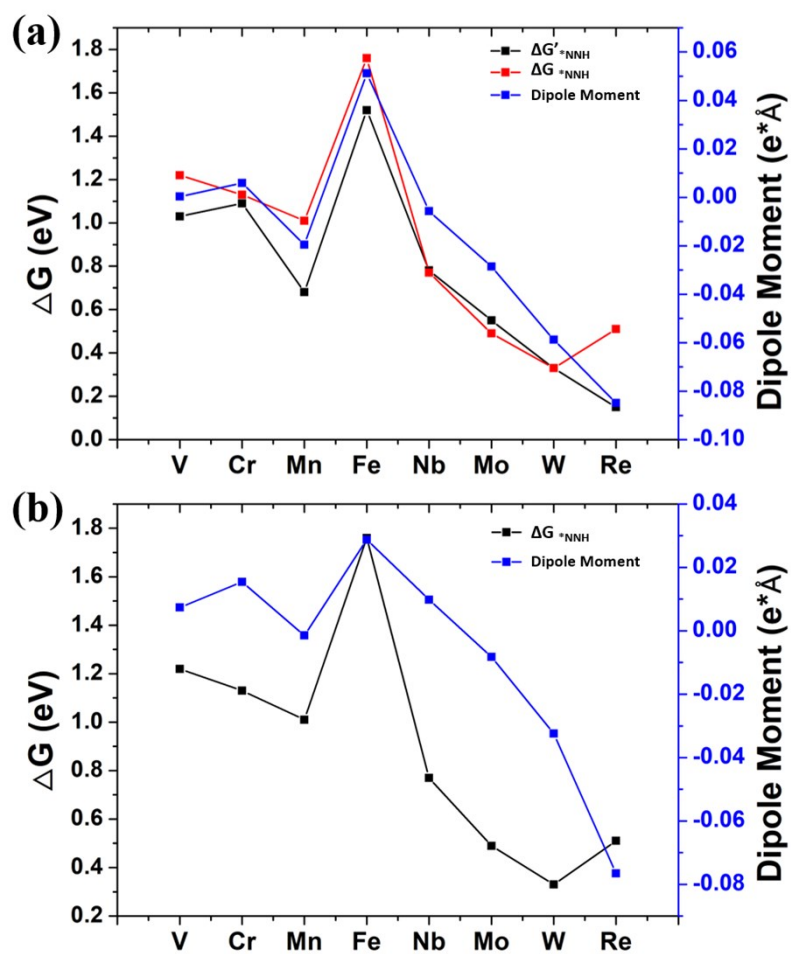
Fig. S11 (a) The relationship between the dipole moments of one adsorbed N_2 and $\Delta G'_{*NNH}$, ΔG_{*NNH}. (b) The relationship between the dipole moments of one of the multi-adsorbed N_2 and the corresponding ΔG_{*NNH}, where the $\Delta G'_{*NNH}$ represents the free energy of $*N_2$ hydrogenation to $*NNH$ and the ΔG_{*NNH} represents the free energy of $*3N_2$ hydrogenation to $*2N_2$-NNH.

Table S13. The atomic charges of supported metals (Q_{TM}) before reaction, the charges accumulated on *H (Q_H) after atomic H adsorbed on the metals with pre-covered multiple N_2, valence electrons (V_{TM}), electronegativity (χ), atomic radius (AR) and electron affinity (EA) of the transition metals.

Coordination	Metal	Q_{TM}	Q_H	V_{TM}	χ	AR	EA
Pyrrolic-N	V	0.5352	-0.0399	5	1.63	171	0.53
	Cr	0.7039	-0.0801	6	1.66	166	0.68
	Mn	0.3998	0.1115	7	1.55	161	0.00
	Fe	0.3293	-0.1171	8	1.83	156	0.16
	Nb	0.9214	-0.1058	5	1.59	198	0.90
	Mo	0.7446	-0.0421	6	2.16	190	0.75
	W	0.5962	-0.0400	6	2.36	193	0.82
	Re	0.4769	0.0124	7	2.93	188	0.16
Pyridine-N	V	0.5814	-0.2321	5	1.63	171	0.53
	Cr	0.6506	-0.0222	6	1.66	166	0.68
	Mn	0.3279	0.1292	7	1.55	161	0.00
	Fe	0.3383	-0.1324	8	1.83	156	0.16
	Nb	0.8784	-0.1446	5	1.59	198	0.90
	Mo	0.6544	-0.0766	6	2.16	190	0.75
	W	0.5141	-0.0692	6	2.36	193	0.82
	Re	0.3951	0.0023	7	2.93	188	0.16

Table S14. The calculated ΔG_{*NNH_DFT}, ΔU_DFT and predicted ΔG_{*NNH_SISSO}, ΔU_SISSO of $V_1(Cr_1, Mn_1, Fe_1, Nb_1, Mo_1, W_1, Re_1)$/pyrrolic-$N_3$-G and $V_1(Cr_1, Mn_1, Fe_1, Nb_1, Mo_1, W_1, Re_1)$/pyridine-$N_3$-G. ($\Delta U = \Delta G_{*M1-H} - \Delta G_{*NNH}$)

	ΔG_{*NNH}_DFT	ΔG_{*NNH}_SISSO	ΔU_DFT	ΔU_SISSO
V_1/pyrrolic-N_3-G	1.22	1.23	0.24	0.25
Cr_1/pyrrolic-N_3-G	1.13	0.93	0.01	0.03
Mn_1/pyrrolic-N_3-G	1.01	1.02	-0.27	-0.27
Fe_1/pyrrolic-N_3-G	1.76	1.73	-0.80	-0.84
Nb_1/pyrrolic-N_3-G	0.77	0.87	-0.08	-0.05
Mo_1/pyrrolic-N_3-G	0.49	0.41	0.19	0.23
W_1/pyrrolic-N_3-G	0.33	0.38	0.24	0.27
Re_1/pyrrolic-N_3-G	0.51	0.47	0.46	0.40
V_1/pyridine -N_3-G	0.89	0.94	-0.63	-0.68
Cr_1/pyridine -N_3-G	0.75	0.78	0.35	0.33
Mn_1/pyridine -N_3-G	1.75	1.78	-0.33	-0.35
Fe_1/pyridine -N_3-G	1.46	1.51	-1.31	-1.24
Nb_1/pyridine -N_3-G	0.43	0.53	-0.26	-0.30
Mo_1/pyridine -N_3-G	0.50	0.55	-0.01	-0.05
W_1/pyridine -N_3-G	0.34	0.29	0.09	0.09
Re_1/pyridine -N_3-G	1.38	1.31	0.39	0.43

Table S15. The calculated ΔG_{*NNH}_DFT, ΔU_DFT and predicted ΔG_{*NNH}_SISSO, ΔU_SISSO on $Nb_1/gt\text{-}C_3N_4$.

	ΔG_{*NNH}_DFT	ΔG_{*NNH}_SISSO	ΔU_DFT	ΔU_SISSO
$Nb_1/gt\text{-}C_3N_4$	0.51	0.40	-0.09	-0.24